Ice accretion simulation on finite wings with extended Messinger Method

S. Özgen[1] & M. Canibek[2]
[1]*Department of Aerospace Engineering,*
Middle East Technical University, 06531, Ankara, Turkey
[2]*Flight Sciences Department, Turkish Aerospace Industries,*
Middle East Technical University Technopolis, 06531, Ankara, Turkey

Abstract

Numerical icing simulations on finite wings are performed using a quasi-3D approach. The solution method consists of computations of the flowfield using the Hess-Smith panel method, droplet trajectories, droplet collection efficiencies, convective heat transfer coefficients and finally ice accretion rates and ice shapes. Inputs to the problem are the ambient temperature T_a, freestream velocity V_∞, liquid water content of air ρ_a, droplet diameter d_p, total icing time t_{exp}, angle of attack α and the wing geometry. Droplet trajectories are calculated by integrating the differential equations of motion for the droplets over time. Droplet impact locations and collection efficiencies are thus determined. Convective heat transfer coefficients are calculated using empirical relations and the solutions of the 2-D integral boundary layer equations. Extended Messinger Method is employed for the prediction of the ice accretion rates. At low temperatures and liquid water contents rime ice occurs and the ice thickness is obtained using an algebraic equation. At higher temperatures and liquid water contents, glaze ice forms for which the energy and mass conservation equations are combined to yield a first order ordinary differential equation, solved numerically. In this case, a thin layer of water is present over a layer of ice and effects of runback water are accounted for. A computer code is developed using the outlined theory, which is validated with experimental ice shapes reported in the literature. Ice shapes are obtained for a wing having taper, twist, dihedral and sweep.
Keywords: ice accretion simulation, Messinger Method, droplet collection efficiency, rime ice, glaze ice.

WIT Transactions on Engineering Sciences, Vol 59, © 2008 WIT Press
www.witpress.com, ISSN 1743-3533 (on-line)
doi:10.2495/AFM080011

1 Introduction

Ice accumulation on parts of the airframe during flight is one of the fundamental problems of aviation. Ice growth on wings, tail surfaces, fuselage, etc. result in severe performance degradation. For example, modification of the wing shape due to ice accumulation results in lift reduction together with increases in drag and weight. Ice formation on control surfaces and stabilizers results in serious and unpredictable degradations in the control characteristics of airplanes. Therefore, it is important to be able to simulate the effects of icing on performance and flight characteristics.

Messinger's study [1] is an important milestone in numerical ice accretion simulation. Increases in capacities and speeds of digital computers in the 1970s allowed theoretical and numerical researchers to analyze realistic geometries such as airfoils, wings and helicopter rotor blades.

In a review paper, Gent *et al*. [2] present the background and the status of analysis developed to address the problem of icing on aircraft. Methods for water droplet trajectory calculation, ice accretion prediction and aerodynamic performance degradation are discussed.

Myers [3] presents a one-dimensional mathematical model describing ice growth, which is an extension of the original Messinger model. It is shown that the model can also be extended to two and three-dimensions and it is the two-dimensional extension that is employed in the current study.

Potapczuk and Bidwell [4] report an effort to develop a three-dimensional ice accretion modeling. Three-dimensional flowfield methods and particle trajectories are combined with two-dimensional ice accretion calculations.

Mingione *et al*. [5] discuss a three-dimensional ice accretion code. Ice accretion on the NASA MS-317 30° swept wing and on the Agusta A109 air intake protection grid are evaluated.

In this article, Section 2 summarizes the approaches used for problem formulation and the solution method. Methods used for computing the flowfield, droplet trajectories, collection efficiencies and convective heat transfer coefficients are explained. Extended Messinger Method is outlined in the same Section. Section 3 is devoted to code validation and presentation of the results. Finally, Section 4 summarizes the study and makes recommendations for future work.

2 Problem formulation and solution method

2.1 Flowfield solution

In order to determine the pressure distribution around the wing and provide the air velocities required for droplet trajectory calculations, 3-D Hess-Smith panel method is employed [6]. The pressure distribution around the wing is also used for boundary-layer calculations in order to determine the convective heat transfer coefficients.

2.2 Droplet trajectories and collection efficiencies

The following assumptions are made for the formulation of the 3-D equations of motion for the water droplets:

- Droplet sizes are small, hence remain spherical,
- The flowfield is not affected by the presence of the droplets,
- Gravity and aerodynamic drag are the only forces involved.

These assumptions are valid for $d_p \leq 500\ \mu m$. The governing equations are:

$$m\ddot{x}_p = -Dcos\gamma_1, \tag{1}$$

$$m\ddot{y}_p = -Dcos\gamma_2, \tag{2}$$

$$m\ddot{z}_p = -(Dcos\gamma_3 + mg), \tag{3}$$

where

$$\gamma_1 = \tan^{-1}\frac{\dot{x_p} - V_x}{V_{rel}}, \quad \gamma_2 = \tan^{-1}\frac{\dot{y_p} - V_y}{V_{rel}}, \quad \gamma_3 = \tan^{-1}\frac{\dot{z_p} - V_z}{V_{rel}}, \tag{4}$$

$$V_{rel} = \sqrt{(\dot{x_p} - V_x)^2 + (\dot{y_p} - V_y)^2 + (\dot{z_p} - V_z)^2}, \tag{5}$$

$$D = 1/2\rho V_{rel}^2 C_D A_p. \tag{6}$$

V_x, V_y and V_z are the flowfield velocity components at the droplet location obtained from the flowfield solution, while $\dot{x_p}$, $\dot{y_p}$, $\dot{z_p}$, $\ddot{x_p}$, $\ddot{y_p}$ and $\ddot{z_p}$ are the components of the droplet velocity and acceleration. A_p is the droplet cross-sectional area. The drag coefficients of the droplets are calculated using the following drag law [2]:

$$\begin{aligned} C_D &= 1 + 0.197Re^{0.63} + 2.6 \times 10^{-4}Re^{-1.34}, \quad Re \leq 3500, \\ C_D &= (1.699 \times 10^{-5})Re^{1.92}, \qquad\qquad\qquad\quad Re > 3500, \end{aligned} \tag{7}$$

where $Re = \rho V_{rel} d_p/\mu$ is the Reynolds number based on droplet diameter d_p and relative velocity V_{rel}. The droplet impact pattern on the wing determines the amount of water that impinges on the surface and the region subject to icing. The local collection efficiency is defined as the ratio, of the area of impingement to the area through which water passes at some distance upstream of the wing. The three-dimensional collection efficiency can be defined as $\beta = A_o/A$, where A_o is the area constituted by four droplets in the release plane, while A is the area of impingement constituted by the same four droplets neighboring a control point. Figure 1 shows the computed particle trajectories and how the collection efficiency is calculated.

2.3 Convective heat transfer coefficients

After flowfield and droplet trajectory calculations, the wing is divided into span-wise strips. Boundary-layer and icing calculations are performed for each of these

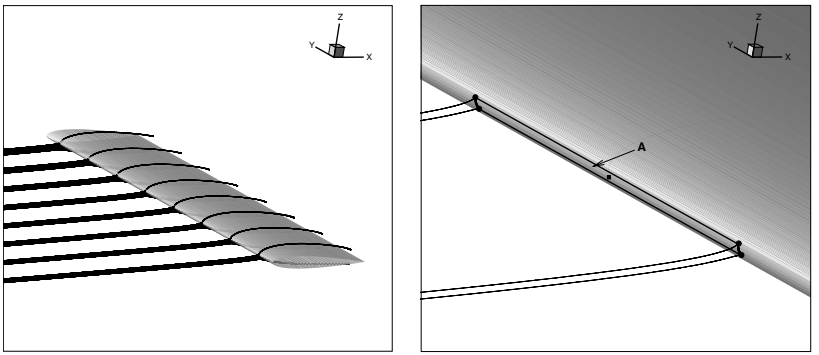

Figure 1: Particle trajectories and collection efficiency calculation.

strips using 2-D approaches. The current study employs a 2-D Integral Boundary Layer Method for the calculation of the convective heat transfer coefficients. With this method, the laminar and turbulent boundary layer properties are calculated fairly accurately provided that the crossflow velocity component due to 3-D effects is not too high compared to the streamwise component. Transition prediction is based on the roughness Reynolds number, $Re_k = \rho U_e k_s/\mu$, where k_s is the roughness height and U_e is the velocity of the external flow at the roughness location. For laminar flow ($Re_k < 600$), formulation of Smith and Spalding is used to calculate the convective heat transfer coefficient [2]:

$$h_c = \frac{0.296 k U_e^{1.435}}{\sqrt{\nu \int_0^s U_e^{1.87} ds}}, \tag{8}$$

where, k is the thermal conductivity of air obtained by assuming constant Prandtl number and viscosity obtained from Sutherland's law as a function of ambient temperature. Streamwise distance along the wing strip starting at the stagnation point is denoted by$s$. For turbulent flow ($Re_k \geq 600$), the method of Kays and Crawford is employed [2]. Accordingly, the turbulent momentum thickness is given by:

$$\theta = \frac{0.036 \nu^{0.2}}{U_e^{3.29}} \left(\int_{s_{tr}}^{s} U_e^{3.86} ds \right)^{0.8} + \theta_{tr}, \tag{9}$$

where θ_{tr} is the laminar momentum thickness at transition location. Skin friction coefficient is found from the Makkonen relation [2]:

$$\frac{C_f}{2} = \frac{0.1681}{[\ln(864\theta/k_s + 2.568)]^2}. \tag{10}$$

The Stanton number can be calculated from [2]:

$$St = \frac{C_f/2}{Pr_t + \sqrt{(C_f/2)/St_k}}. \tag{11}$$

The roughness Stanton number is calculated from [2]:

$$St_k = 1.92 Re_k^{-0.45} Pr^{-0.8}. \tag{12}$$

Finally, turbulent convective heat transfer coefficient is found from [2]:

$$h_c = St \rho U_e C_{pa}. \tag{13}$$

The roughness height is calculated from $k_s = 0.00117 K_{V_\infty} K_{LWC} K_{T_a} K_{d_p} \bar{c}$, where K_{V_∞}, K_{LWC}, K_{T_a} and K_{d_p} are empirical factors accounting for freestream velocity, liquid water content, ambient temperature and droplet size effects [7]. The mean aerodynamic chord of the wing is denoted by $\bar{c}$.

2.4 Extended Messinger method

Icing prediction is based on phase change or the Stefan problem. The Stefan problem is governed by four equations: heat equations in the ice and water, a mass balance and a phase change condition at the ice/water interface [3]:

$$\frac{\partial T}{\partial t} = \frac{k_i}{\rho_i C_{pi}} \frac{\partial^2 T}{\partial y^2}, \tag{14}$$

$$\frac{\partial \theta}{\partial t} = \frac{k_w}{\rho_w C_{pw}} \frac{\partial^2 \theta}{\partial y^2}, \tag{15}$$

$$\rho_i \frac{\partial B}{\partial t} + \rho_w \frac{\partial h}{\partial t} = \rho_a \beta V_\infty + \dot{m}_{in} - \dot{m}_{e,s}, \tag{16}$$

$$\rho_i L_F \frac{\partial B}{\partial t} = k_i \frac{\partial T}{\partial y} - k_w \frac{\partial \theta}{\partial y}, \tag{17}$$

where θ and T are the temperatures, k_w and k_i are the thermal conductivities, C_{pw} and C_{pi} are the specific heats and h and B are the thicknesses of water and ice layers, respectively. In equation (16), $\dot{m}_{in}$ and $\dot{m}_{e,s}$ are runback and evaporating (or sublimating) water mass flow rates, respectively. On the other hand, ρ_i and L_F denote the density of ice and the latent heat of solidification of water, respectively. Ice density is assumed to have different values for rime ice, ρ_r and glaze ice, ρ_g. The coordinate y is normal to the surface. In order to determine the ice and water thicknesses together with the temperature distribution at each layer, boundary and initial conditions must be specified. These are based on the following assumptions:

- Ice is in perfect contact with the wing surface (surface temperature is assumed to be equal to the ambient temperature, $T_s = T_a$):

$$T(0, t) = T_s. \tag{18}$$

- The temperature is continuous at the ice/water boundary and is equal to the freezing temperature, T_f:

$$T(B,t) = \theta(B,t) = T_f. \tag{19}$$

- At the air/water (glaze ice, $y = B+h$) or air/ice (rime ice, $y = B$) interface, heat flux is determined by convection $Q_c = h_c(T_s - T_a)$, heat from incoming droplets $Q_d = \rho_a \beta V_\infty C_{pw}(T_s - T_a)$, heat brought in by runback water $Q_{in} = \dot{m}_{in} C_{pw}(T_f - T_s)$, evaporation $Q_e = \chi_e e_o(T_s - T_a)$ or sublimation $Q_s = \chi_s e_o(T_s - T_a)$, aerodynamic heating $Q_a = r h_c {V_\infty}^2/2C_{pa}$, kinetic energy of incoming droplets $Q_k = \rho_a \beta {V_\infty}^3/2$, and latent heat release $Q_l = \rho_r L_F \partial B/\partial t$:

$$\begin{aligned} \text{Glaze ice} &: -k_w \frac{\partial \theta}{\partial y} = (Q_c + Q_e + Q_d) - (Q_a + Q_k + Q_{in}), \\ \text{Rime ice} &: -k_i \frac{\partial T}{\partial y} = (Q_c + Q_s + Q_d) - (Q_a + Q_k + Q_{in} + Q_l). \end{aligned} \tag{20}$$

  Evaporation and sublimation coefficients are expressed as:

$$\chi_e = \frac{0.622 h_c L_E}{C_{pa} P_t Le^{2/3}}, \quad \chi_s = \frac{0.622 h_c L_S}{C_{pa} P_t Le^{2/3}}, \tag{21}$$

  and P_t is the total pressure of the freestream flow.
- The wing surface is initially clean:

$$B = h = 0, \quad t = 0. \tag{22}$$

2.4.1 Rime ice growth and temperature profile

Rime ice thickness follows from the mass balance in equation (16), since water droplets freeze entirely on impact:

$$B(t) = \frac{\rho_a \beta V_\infty + \dot{m}_{in} - \dot{m}_s}{\rho_r} t. \tag{23}$$

2.4.2 Glaze ice growth

Glaze ice thickness is obtained by time-integration of the ordinary differential equation obtained by combining mass and energy equations:

$$\rho_g L_f \frac{\partial B}{\partial t} = \frac{k_i(T_f - T_s)}{B} + k_w \frac{(Q_c + Q_e + Q_d) - (Q_a + Q_k)}{k_w + h(Q_c + Q_e + Q_d)/(T_s - T_a)} - Q_{in}. \tag{24}$$

It is assumed that, all unfrozen water runs back to the neighboring downstream cell for the upper surface, while all water sheds for the lower surface [8]. To calculate the glaze ice thickness, equation (24) is integrated numerically, using a Runge–Kutta–Fehlberg method. Water layer thickness for glaze ice conditions is found

Table 1: Parameter values used in the calculations.

Symbol	Definition	Value
C_{pa}	Specific heat of air	1006 J/kg.K
C_{pi}	Specific heat of ice	2050 J/kg.K
C_{pw}	Specific heat of water	4218 J/kg.K
e_o	Saturation vapor pressure constant	27.03
g	Gravitational acceleration	9.81 m/s^2
k_i	Thermal conductivity of ice	2.18 W/m.K
k_w	Thermal conductivity of water	0.571 W/m.K
Le	Lewis number	$1/Pr$
L_F	Latent heat of solidification	3.344×10^5 J/kg
L_E	Latent heat of evaporation	2.5×10^6 J/kg
L_S	Latent heat of sublimation	2.8344×10^6 J/kg
Pr	Laminar Prandtl number of air	0.72
Pr_t	Turbulent number of air	0.9
r	Adiabatic recovery factor	1/2: laminar flow 1/3: turbulent flow
μ_w	Viscosity of water	1.795×10^{-3} Pa.s
ρ_r	Density of rime ice	880 kg/m^3
ρ_g	Density of glaze ice	917 kg/m^3
ρ_w	Density of water	999 kg/m^3

from the following expression:

$$h = \frac{(\rho_a \beta V_\infty + \dot{m}_{in} - \dot{m}_e)}{\rho_w}(t - t_g) - \frac{\rho_g}{\rho_w}(B - B_g). \tag{25}$$

where B_g is the rime ice thickness at which glaze ice first forms, and t_g is the corresponding time given as:

$$B_g = \frac{k_i(T_f - T_s)}{(\rho_a \beta V_\infty + \dot{m}_{in} - \dot{m}_s)L_F + (Q_a + Q_k + Q_{in}) - (Q_c + Q_e + Q_d)}, \tag{26}$$

$$t_g = \frac{\rho_r}{(\rho_a \beta V_\infty + \dot{m}_{in} - \dot{m}_s)} B_g. \tag{27}$$

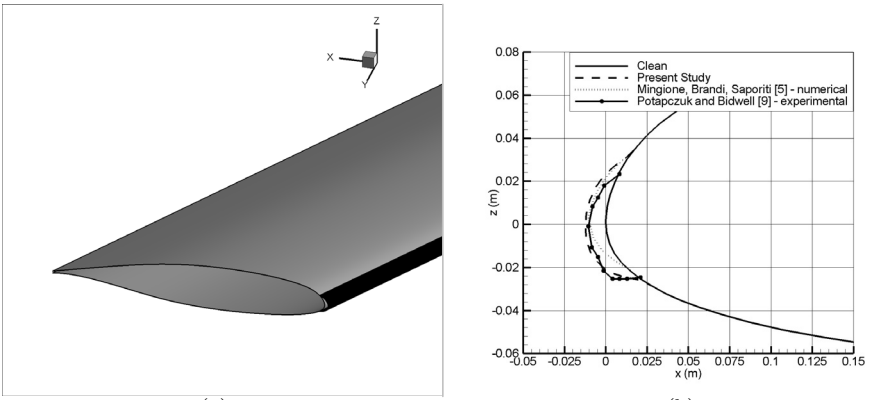

(a) (b)

Figure 2: Ice shapes on a 30° swept wing having NASA MS-317 section.

Table 2: Icing conditions for the cases presented in Figures 2 and 3.

Variable	**Value (Figure 2)**	**Value (Figure 3)**
Angle of attack, α	0°	4°
Freestream velocity, V_∞	74 m/s	129 m/s
Wingroot chord length, c_r	0.9 m	1 m
Wing span, b	7.3 m	8 m
Taper ratio, λ	1	0.5
Leading edge sweep, Λ_{le}	30°	10°
Dihedral angle, Γ	0°	4°
Geometric twist, θ	0°	4°
Ambient temperature, T_a	$-18.1°C$	$-12.6°C$
Exposure time, t_{exp}	390 s	120 s
Droplet size, d_p	20 μm	20 μm
Liquid water content, ρ_a	1 g/m^3	1 g/m^3

3 Validation of the method, results and discussion

Figure 2 shows the ice shapes and comparisons with numerical and experimental data in the literature for a 30° swept NASA MS-317 wing. Icing and geometrical conditions for this case are given in the second column of Table 2. As can be seen, a typical rime ice shape is obtained and it is in very good agreement with the experimental and the numerical ice shapes reported in the literature. Also, the extent of the iced region is well predicted.

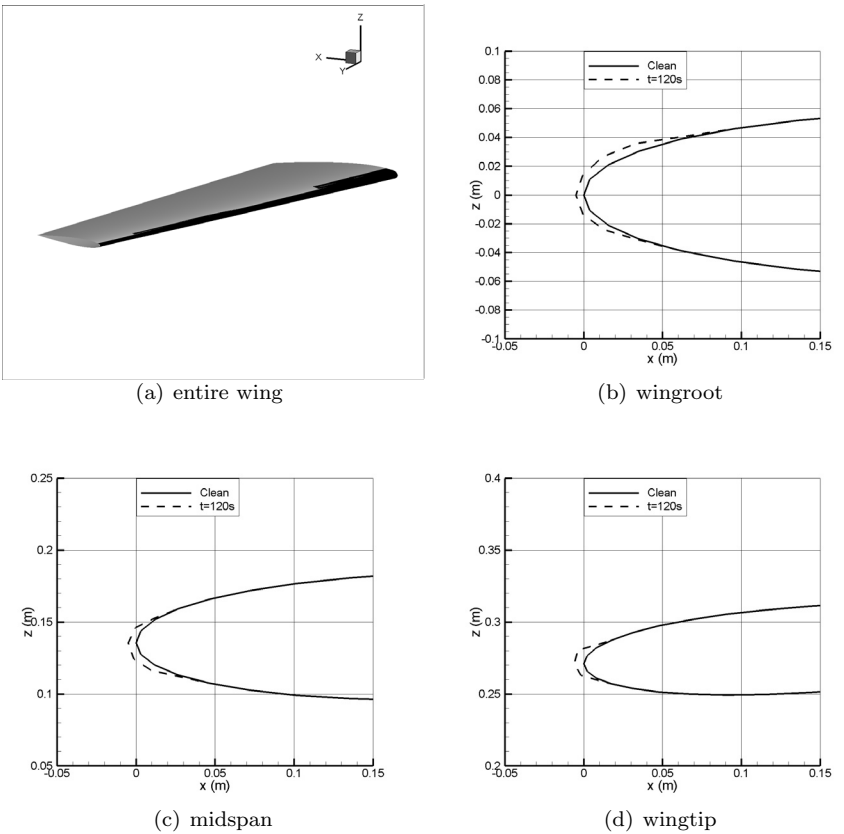

(a) entire wing (b) wingroot

(c) midspan (d) wingtip

Figure 3: Ice shapes on a 10° swept wing having NACA 0012 section.

Figure 3 shows the results for a wing with taper, twist, dihedral and sweep having NACA 0012 section. This wing is representative of wings that one would see on real airplanes. Icing and geometrical conditions for this case are given in the third column of Table 2. As expected, there is a spanwise variation of both the ice thickness and the iced region. At the wingroot, the ice is thin but extends through a wide portion of the leading edge. On the other hand, at the wingtip, the ice is thicker but is confined to a narrower region of the leading edge. These inferences are in qualitative agreement with the results reported by Özgen *et al*. [9]. As reported in [9] smaller wing sections yield higher collection efficiencies, hence leading to thicker and more severe icing. The ice shape in Figure 3b suggests that there is glaze ice formation, at least on some parts of the wing.

4 Conclusions and recommendations for future work

Ice accretion predictions on finite wings have been performed using a quasi-3D approach. Results indicate that the strip approach is capable of predicting ice

shapes with success, although the boundary-layer and thermodynamical models used are 2-D. The tool can be used for preliminary design purposes for the selection of a de/anti-icing system or for certification.

The current tool can be developed to a full 3-D code by implementing a 3-D boundary-layer solver and a thermodynamical model. This will be at the expense of computational complexity and increased run time. Then, the user has to decide what to use such a tool for and trades between simplicity, good accuracy versus complexity, improved accuracy need to be considered. However, if more complex geometries like intakes or highly swept wings are to be studied, then these improvements are almost imperative. As a further improvement, a more sophisticated liquid water model can be introduced, like those described by Fortin *et al*. [8] and Myers *et al*. [10].

References

[1] Messinger, B., Equilibrium temperature of an unheated icing surface as a function of airspeed. *Journal of Aeronautical Sciences*, **January 1953**, pp. 29–42, 1953.
[2] Gent, R., Dart, N. & Cansdale, J., Aircraft icing. *Phil Trans R Soc Lond A*, **358**, pp. 2873–2911, 2000.
[3] Myers, T., Extension to the Messinger model for aircraft icing. *AIAA J*, **39**, pp. 211–218, 2001.
[4] Potapczuk, M. & Bidwell, C., Swept wing ice accretion modeling. Technical report, NASA TM–103114, 1990.
[5] Mingione, G., Brandi, V. & Saporiti, A., A 3d ice accretion simulation code. AIAA Paper 99-0247, 1999.
[6] Katz, J. & Plotkin, *Low-Speed Aerodynamics*. Springer-Verlag: Berlin and New York, pp. 11–13, 1984.
[7] Wright, W., Genat, R. & Guffond, D., Dra/nasa/onera collaboration on icing research part ii, prediction of airfoil ice accretion. Technical report, NASA CR–202349, 1997.
[8] G. Fortin, J.L.L. & Ilinca, A., Heat and mass transfer during ice accretion on aircraft wings with an improved roughness model. *Int J Thermal Sciences*, **45**, pp. 595–606, 2006.
[9] Özgen, S., Ortakaya, Y. & Korkem, B., Ice accretion simulation on multi-element airfoils. *Proc. of the 2nd European Conf. for Aerospace Sciences*, Brussels, 2007.
[10] Myers, T., Charpin, J. & Thompson, C., Slowly accreting ice due to supercooled water impacting on a cold surface. *Physics of Fluids*, **14**, pp. 240–256, 2002.